Chromatic Monitoring of Gear Mechanical Degradation based on Acoustic Emission

M. Delgado-Prieto, *Member, IEEE* and D. Zurita-Millán, *Student Member, IEEE*

***Abstract*— This paper presents a methodology for the feature estimation of a new fault indicator focused on detecting gear mechanical degradation under different operating conditions. Preprocessing of acoustic emission signal is performed by applying chromatic transformation to highlight characteristic patterns of the mechanical degradation. In this work, chromaticity based on the computation of the HLS transformation of the main acoustic emission intrinsic mode functions is performed. Then, a topology preservation approach is carried out to describe the chromatic signature of the healthy gear condition. Thus, the detection index can be estimated. It must be noted that the applied chromatic monitoring process only requires the characterization of the healthy gear condition, being applicable to a wide range of operating conditions of the gear. Performance of the proposed system is validated experimentally. According to the obtained results the proposed methodology is reliable and feasible for monitoring gear mechanical degradation in industrial applications.**

***Index Terms*— Acoustic signal processing, Acoustic testing, Chromatic monitoring, Fault detection, Frequency-domain analysis, Gears.**

Manuscript received March 21, 2016; revised May 2, 2016; August 31, 2016 and March 6, 2017; accepted April 23, 2017.

This work was supported in part by the MINECO, Spain, under the Project CICYT TRA2013- 46757-R, and the Generalitat de Catalunya, GRC MCIA, Grant SGR 2014-101.

M. Delgado-Prieto and D. Zurita-Millán are with the department of Electronic Engineering, Technical University of Catalonia (UPC), MCIA Research Center, Rbla. San Nebridi 22, 08222 Terrassa, Spain (phone: +34-93-739-8518; fax: +34-93-739-8972; e-mails: miguel.delgado@mcia.upc.edu, daniel.zurita@mcia.upc.edu).

I. INTRODUCTION

DURING the last years, the diagnosis procedures are being particularly oriented beyond the electrical motor. Indeed, mechanical components such as gears, external bearings or screw shafts, among others, are critically important for a proper operation of the machinery [1]. The faulty condition of a mechanical component, even external to the electrical machine, represents a triggering factor that leads to the propagation of secondary damages due to the continued operation. The most common failures, dealing with industrial machinery, are those related with the power transmission chain [2]. The gearbox is found to be the most critical part since its downtime per failure is usually critical in comparison to other components [3]. It is for this reason that gearbox condition monitoring is of significant importance to reduce failures and to assure the continuity of machinery operation. A research effort is required to achieve monitoring procedures specifically designed to estimate fault indicators for gear- based drives.

Dealing with mechanical fault detection, vibration monitoring is one of the most common approaches [4], [5], however, acoustic emission (AE), shows three important advantages [6], [7]. First, AE sources are non-directional, which reduces the number of required sensors. Second, AE is produced from microscopic levels, which allows the detection of mechanical fractures at earlier stages. Third, AE implies higher elastic wave frequency, which avoids structural resonances and mechanical background noise. In rotating gearboxes, AE is produced by the load transmission due to the contact of gears in relative motion. Thus, a surface or subsurface crack initiation leads to a rapid release of strain energy caused by a structural alteration that produces elastic wave emission. During a mechanical fracture procedure, three different phases are commonly identified: initiation, incubation and propagation. Different studies on metallic materials tribology shown that, in presence of fractures, the AE events exhibit an amplitude increase as well as a different distribution of the frequency content. This effect is analyzed in works such as the presented by E. Martinez-Gonzalez *et al.* in [8], [9], and Z. Shi *et al.* [10], where the correlation of the AE

signature in regard with the mechanical fracture phases is studied. Thus, as the fracture evolves, the effects are more evident, until can be detected by mechanical vibration based frequency transducers. Indeed, other approaches such as vibrations, temperatures or stator currents based are limited to the detection of advanced fracture propagation stages.

Research towards gear mechanical degradation monitoring schemes by means of AE has been carried out by several authors. Elforjani *et al.* [11] compared the applicability of AE and vibration technologies in detecting defects on worm gears by means of statistical-time features. The results showed that the AE-based approach was more reliable, robust and sensitive to the detection of defects than the vibration based monitoring scheme. Similar approach is presented by Tan *et al.* [12]. In [13], Li and He presented a methodology for gear health monitoring in rotational machinery. The diagnosis scheme is divided in two major steps, the incorporation of a threshold-based denoising technique into Empirical Mode Decomposition (EMD), and the estimation of multiple statistical-time features from the resulted signal, which are fused later in a singular feature for healthy states identification. The method reaches reliable tooth root crack detection, but it does not face the effect of the speed variation over the proposed fault indicator. In [14], the authors dedicated their effort in the estimation of kurtosis and crest factor of the resulting EMD time-domain acoustic signals to determine the conditions of bearings and gears. It was found that the methodology is very effective, but the interpretation of the severity damage is not obvious. Some authors as Eftekharnejad *et al.* [15], focused their efforts to decompose the signal into several frequency ranges thereby achieving better understanding of the frequency content of the signal. The frequency spectrum of AE signatures at various wavelet decomposed levels showed variations during different stages of the fracture. In this kind of analysis, the fault indicators extracted from thresholding the energy across different frequency bands are the most used ones. However, the energy values extracted are directly used in fault classification systems in order to be processed with the rest of parameters, and not previously analyzed in order to extract a fault indicator which contains fault detection information itself, as it is proposed in this study. Indeed, the main drawback of these methods is related with both the use of

statistical time based fault indicators, which directly affects the effectiveness of identifying the fault patterns hidden within the dynamic signals [16], and the lack of a common framework able to be applied simply in a range of speed operating regimes to interpret the condition of the component under test.

In this paper, partially damaged gears which operate under different speed conditions are studied. For this objective, the AE signals are, first, decomposed in the main intrinsic mode functions (IMF). Then, the chromatic estimation by HLS transformation is proposed to obtain a high-dimensional chromaticity space describing the healthy gear operation. Next, a neural network based topology preservation scheme is proposed to describe such chromaticity space. Finally, a reliable and low computational cost parameter is proposed to detect mechanical gear degradation by quantifying chromatic deviations.

The contribution of this study lies in a new feature estimation methodology, and the verification of the chromatic theory capabilities for fault gear detection based on AE signal analysis. A high-resolution chromaticity space by means of EMD has been chosen in order to check the proposed fault indicator when different speed operating regimes and fault severity conditions take place. The use of a self-organizing map (SOM), as topology preservation technique, allows the exploration of the high-dimensional chromaticity space for interpretation and visualization purposes. Indeed, this approach allows the preservation and analysis of the underlying physical phenomenon of the mechanical degradation.

Novelties of this work include a new fault detection method based on the AE signal decomposition, their chromatic transformation, and the spectral contents analysis and characterization through a topology preservation map. Note that it is the first time that this methodology as well as this gear mechanical degradation indicator is used in electromechanical systems for mechanical gear fault detection.

This paper is organized as follows. The theoretical basis and overview of chromatic monitoring and HLS transformation is presented in Section II. The novel feature estimation methodology, including empirical mode decomposition, topology preservation and fault indicator calculation are explained in Section III. The experimental set-up is explained in Section IV. Competency of the method and experimental results are discussed in section V. Finally, conclusions are shown in Section VI.

II. HLS TRANSFORMATION

The chromatic analysis is based on the interpretation of applying different receptors partially superposed over a signal [17], [18], like human perception. The resulting parameters are, then, interconnected between them, which allow a smooth behavior of their response. However, this approach requires a different methodology for information assimilation and representation. Thus, the chromatic monitoring is considered as a balanced distribution between the estimation of signal characteristics and condition interpretation and visualization [19]. The chromatic methodology is based upon comparisons, which are translated into mathematical cross correlations. Thus, to extract meaningful information from the outputs of a set of receptors, chromaticity theory transforms them into mathematical forms that can emphasize and distinguish particular information. Indeed, Stergioulas *et al.* [20], demonstrated that three chromatic processors are capable of discriminating approximately 95% of considered signals following a Gabor's representation. The Gabor expansion can be implemented as a Gabor analyzer in a way analogous to a spectrum analyzer that performs a Fourier analysis in terms of sinusoidal signals. Filters with gaussian response (Gabor filters), evaluated over the signal result in Gabor coefficients. Such coefficients have been demonstrated to be highly reliable in the reconstruction of an objective signal, $x(t)$, following a von Neumman's lattice subsets approach of Gaussian signals, $r(t;A,\rho)$, such as:

$$x(t) = \sum_{m=1}^{M} \sum_{n=1}^{N} \frac{1}{\pi} S_{mn}(\rho) r(t; A, \rho) \tag{1}$$

where $S_{mn}(\rho)$ represents an array of coefficients, A is a discretized complex number defined as $m\alpha_1 + jn\alpha_2$ in the von Neumann's lattice subset consideration, where m and n are integer numbers and α_1 and α_2 define the von Neuman's lattice cell area, and the Gaussian shape parameter ρ a fixed value greater than 0. Considering, for example, a random signal in frequency, $x(f)$, the chromaticity theory considers three signal receptors, R, G and B, that is, Gabor filters. Fig. 1(a) shows the classical gaussian-shaped chromatic processor profiles.

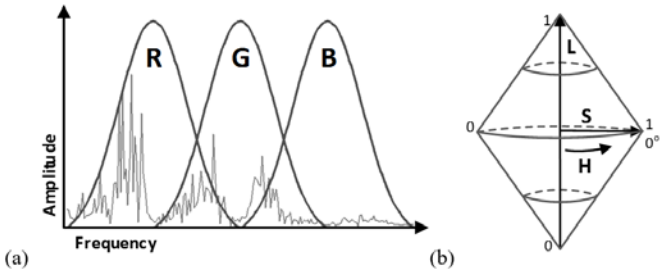

Fig. 1. HLS transformation. a) Non-orthogonal receptors applied over a spectral response of a signal. b) Chromatic parameters representation.

The receptors *R*, *G* and *B* correspond to filter structures, which determine the sensitivity throughout the frequency range and provides three chromatic values, Gabor's coefficients, classically named as red, green, and blue. Instead of a signal reconstruction scheme, in this study is proposed the transformation of such information into chromatic parameters in order to characterize and distinguish among different signals. There are many transformations well established in the literature, however, the HLS transformation (Hue, Light and Saturation), represents a good trade-off between simplicity and performance. The transformation is done as follows:

$$H = \begin{cases} 240 - 120 \cdot \left(\frac{g}{g+b}\right) \; if \; r = 0 \\ 360 - 120 \cdot \left(\frac{b}{b+r}\right) \; if \; g = 0 \\ 120 - 120 \cdot \left(\frac{r}{r+g}\right) \; if \; b = 0 \end{cases} \tag{2}$$

$$L = \frac{R+G+B}{3} \tag{3}$$

$$S = \frac{max(R,G,B) - min(R,G,B)}{max(R,G,B) + min(R,G,B)} \tag{4}$$

where $r = R\text{-}min(R, G, B)$, $g = G\text{-}min(R, G, B)$ and $b = B\text{-}min(R, G, B)$. Thus, *H*, the hue, characterizes the frequency contents in an angle range from 0º to 360º, i.e. low values of *H* imply low frequency contents while high values of *H* correspond to high frequency contents. The *L*, the lightness, represents the intensity

in a range from 0 to 1, i.e. low values of *L* correspond to a limited content, while high values of *L* correspond to an elevated content. Finally, the *S*, the saturation, characterizes the dominating frequency in a range from 0 to 1, i.e. low values of *S* correspond to signals with wide spectral content, while high values of *S* correspond to signals with narrow spectral content. Thus, the values resulting from the HLS transformation represent an equivalent chromatic representation of which the original signal is member, as shown in Fig. 1(b). Thus, such chromatic approach allows a simple and powerful characterization of signals. The chromatic parameters are proposed to be advantageous in order to detect the presence of mechanical gear degradation.

III. Chromatic Monitoring Methodology

The estimation of numerical features is a crucial step in most pattern recognition problems. This fact is, mainly, due to the irrelevant information or noise usually contained in the raw input data. Indeed, the features must be chosen accordingly to a particular application, which determines the requirements of the information to be extracted. However, in numerous occasions the amount of available data is too large, requiring an important computational burden. Taking into account such circumstances it is suitable to apply comprehensive and optimized pattern recognition schemes in general, and enhanced feature estimation procedures in particular. This allows retaining as much as possible the relevant information contained in the raw input data in a reduced set of parameters easily recognizable by a fault detection procedure. Dealing with gear mechanical degradation by means of AE, it must be taken into account that the AE activity increases with the mechanical fracture, as well as the presence of additional frequency bands during the earlier stages of the mechanical degradation [21]. Thus, the chromatic approach, that is, the estimation and analysis of hue, lightness and saturation is highly aligned with the mechanical fracture effects over the AE signal, since the amplitude and frequency distribution are characterized. The chromatic monitoring methodology proposed in this work involves five sequential steps, first, the decomposition of the acquired AE signal in intrinsic mode functions in order to identify main oscillatory frequency modes. Second, the

application of the chromatic processors to obtain Gabor's coefficients (*R*, *G* and *B*). Third, the generation of a *D*-dimensional chromaticity space by means of the HLS transformation over the obtained *R*, *G* and *B* coefficients of each considered intrinsic mode function. Such chromaticity space will contain, then, the complete description of the AE signal acquired during the healthy gear condition characterization. Fourth, the chromaticity space mapping by means of a topology preservation based technique. And, fifth, the estimation of the proposed fault indicator by the assessment of new AE measurements over the mapped chromaticity space. The complete proposed detection methodology is represented in Fig. 2.

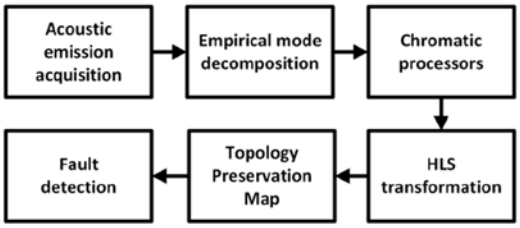

Fig. 2. Proposed fault detection methodology.

A. Acoustic decomposition process

Classical AE approaches applied to mechanical degradation analysis are based on AE events counting by thresholding the signal [22]. These methods have been proved to be useful under controlled metallographic samples analysis at laboratory scale. Dealing with industrial electromechanical machinery, the temporal AE signal is subjected to variability due to the operating set point or oscillatory load modes among others. Thus, the analysis of the spectral content becomes in a significant alternative in order to estimate the mechanical degradation [23]. The classical spectral analysis (Fourier transform), allows splitting a time-signal into its individual frequencies by computing the relative strength of each component. However, one drawback of the Fourier transform is that it may mask failure related components that appear in a given time instant and are of a very short duration in regard with the temporal window used for the Fourier transform calculation. This is the case in gear teeth degradation analysis, where the presence of a fractured

tooth will be only significantly reflected in those AE events collected during the stress of the corresponding gear tooth, i.e. once per gear rotation in regular spur gears. In this sense, different signal decomposition approaches are being the most promising strategies to be applied for AE analysis. The main drawbacks of these methods are related with the frequency ranges to be included in each sub-signal. In particular, the IMF estimation is considered as a good balanced decomposition due to its signal adaptive capabilities. The IMF represent oscillatory modes, but are much more general than harmonic functions. In fact, it is worth noting that the IMF are modulated both in amplitude and in frequency and, consequently, are not restricted to be stationary. The EMD method extracts, from a given time based signal, *x(t)*, the M number of IMF by the so called shifting process [24]. The obtained *imf(k) ,k=1..M*, can be reassembled in order to obtain the original data as follows:

$$x(t) = \sum_{k=1}^{M} imf_k(t) + r_M(t) \tag{5}$$

where $r_M(t)$, the last residue, is a constant or a monotonic function which represents the general trend of the time series. Indeed, the EMD models a signal as a sum of oscillatory components (IMFs), formed by narrow spectral bands. Thus, the EMD gives the evolution of such frequency bands along the considered time window [25]. Current approaches suggest discarding the less contributive IMF, usually related with uncertainties and non-significant modes. In the proposed methodology, for each considered intrinsic mode function three chromatic processors are applied, and the corresponding HLS transformation is carried out to obtain a *D*-dimensional chromaticity space.

B. Chromaticity space mapping

Feature reduction methods have been applied in the last years to preserve and characterize the information in a lower *d*-dimensional space, where *D>d*. The feature reduction process has been typically implemented with linear techniques such as Principal Component Analysis (PCA). However, PCA has been discussed by many authors emphasizing its limitation dealing with large data sets, because it seeks for a

global structure of the data [26]. Concerning with this problem manifold learning methods has been applied in the last years [27]. Among them, the self-organizing map is the most used, which is based on developing a neural network grid to preserve most of the original distances between feature vectors in the *D*-space into a *d*-dimensional output space. The output space is predefined as a regular *d*-dimensional grid, usually *d*=2 for visualization purposes. Each point in the grid represents a neuron. For each neuron ne_i, a *D*-dimensional weight vector wv_j is defined. The weights represent the neurons' position in the input space. Mapping is performed by assigning each data point xv_i in the input space to one of these neurons, namely the one whose weight vector is closest to the point. The position vector yv_i in the output space of such data point is, then, given by the grid position of this neuron. A schematic representation of the SOM performance is shown in Fig. 3. During the training of the topology preservation map, the used error function corresponds as follows:

$$E_{SOM} = \sum_{j} \sum_{i \in s_{yi}} \left(w_{vj} - x_{vi}\right)^2 \tag{6}$$

with $s_{y\text{-}i}$ being the set of data points which have neuron i as closest neuron. E_{SOM} expresses the average squared distance from a point in the original *D*-dimensional space to its representative neuron. The minimization of E_{SOM} represents the objective of the operation, and is performed with respect to the weight vectors $w_{v\text{-}j}$. Thus, the feature reduction procedure is applied to highlight and characterize patterns.

The proposed method is based on the detection of deviations in regard with the chromatic signature of the healthy gear condition. The topology preservation approach conserves the topology properties of the data to be mapped, which allows the interpretation of the underlying physical phenomena described by the chromaticity space.

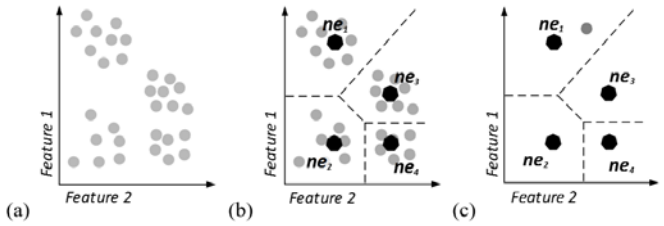

Fig. 3. Self-organizing mapping procedure in a 2-dimensional input space. (a) Representation of a 2-dimensional set of measurements. (b) Resulting 2-dimensional positioning of a predefined set of four neurons. During the training process, the neurons minimize a topology preservation error by improving their position. The dotted lines represent boundaries of the input space regions related to each neuron considering the regular Euclidian distance. (c) Example of a new measurement assessment. In this case, the shortest distance corresponds to ne1, then, the corresponding ne_1 weight vector will be applied to project the sample in the resulting *d*-dimensional space.

C. Damage assessment

The collection *a priori* of data corresponding to damaged gears is a critical matter in most of practical applications. Thus, the proposed methodology has been envisaged in order to be initialized only with the healthy conditions. Then, the data corresponding to the healthy scenarios is characterized in a *d*-dimensional map. Similar AE measurements will exhibit short distances to the map, which reflect the healthy behavior. AE deviations, however, will show larger distances. That is, AE samples containing faulty gear patterns, characterized by means of the chromatic parameters, will be projected far from the neurons' map. For this purpose, a healthy threshold, *Ht*, is defined. The number of AE measurements over the threshold as well as their distances to the nearest neuron, are considered as a representative metric of the fault severity level (7). Then, the proposed gear mechanical degradation indicator, I_{GMD}, includes not

only the identification of characteristic AE healthy/faulty patterns, but also the assessment of the severity degree.

$$I_{GMD} = \frac{\sum_{i=1}^{M} \sqrt{\sum_{j=1}^{D} \left(x_j^i - y_j^i\right)^2}}{M} \tag{7}$$

where *M* means the number of measurements which distances to their closest neuron are bigger than the threshold condition, *D* corresponds to the chromaticity space dimensionality, *x* the measurement and *y* the corresponding closest neuron to the measurement projection.

IV. Experimental Results

The experimental set-up is based on two permanent magnet synchronous machines, PMSMs, acting as a drive and load connected to a 1:1 rated gearbox by means mechanical couplings. The motors respond to 3 pair of poles at 6000 rpm and 2.3 Nm of rated speed and torque respectively. A commercial AE transducer, Vallen-Systeme VS900-M, covering the spectral band of interest from 50 kHz to 500 kHz, is located in contact with the gearbox casing as close as possible to the shaft as proposed in similar works [28], [29]. Data acquisition is done with DAQ NI PXI 6115, a multifunction board up to 10Msamples/s and 12 bits of resolution.

Three different rotating speeds conditions at half-rated load have been considered: 150 rpm, 250 rpm and 450 rpm. Thus, the load motor is commanded by a half-rated torque set point, while the drive motor is commanded by one of the three speed set-points considered. Three gears have been used to carry out the methodology validation, a healthy gear, *He*, a faulty gear with 4 fractures induced on the base corners of four teeth (sized between 1mm and 2mm), *Fa*, and another faulty gear with fractures induced along the base of four teeth (sized around 5mm), *Fb*. The fractures, over 31-teeth F114 steel gears, have been carried out by mechanical fatigue tests. It must be noted that fracture tooth represents a challenging mechanical gear fault scenario [30]. Thus, by means of laboratory testing machinery, gears were subjected to fatigue cycles until the elastic module of the material was reached and a fracture appeared. The tests were stopped

once cracks were evidenced macroscopically and, then, measured. Once the gears were submitted to the fatigue tests they were mounted in the rotating test bench for AE acquisition. The electromechanical experimental setup and the set of gears are shown in Fig. 4 and Fig. 5 respectively. The sampling frequency is fixed at 2 MHz. A total amount of 20 ksamples are acquired, that is, each acquisition corresponds to 10 msec. of AE signal. For each experimental condition analyzed, a total acquisition time of 10 sec. has been carried out.

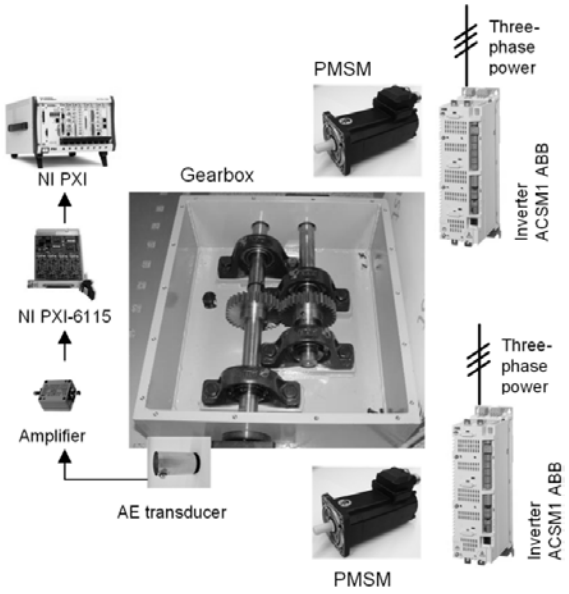

Fig. 4. Experimental setup for mechanical gear fault detection formed by two PMSMs controlled by independent inverters, a gearbox, an AE transducer and the acquisition card.

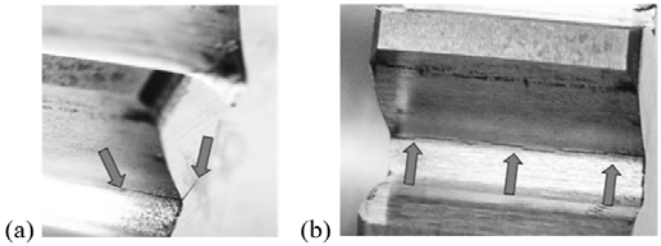

Fig. 5. Mechanical gear fractures induced. (a) Example of one of the fractures at the corner base of a gear tooth, fault *Fa*. (b) Example of one of the fractures along the base of a gear tooth, fault *Fb*.

A. Competency of the method

Previously to the evaluation of the proposed methodology, the performance of a classical AE event thresholding approach has been analyzed. Thus, considering the healthy gear records, thresholds from 25% to 90% of the maximum AE event have been applied. The resulting counting values are shown in Fig. 6. Indeed, the speed increase implies an excitation stress intensification resulting from the tooth contact. Such effect means a gain in the AE activity and, consequently, longer AE event decays. This behavior is clearly manifest in the AE signal thresholding analysis, where the number of AE counts increases with the speed. However, although most of the thresholds exhibit AE counts bigger than the obtained under the corresponding healthy gear condition, it is not possible to select one to distinguish among the nine experimental tests. Then, the AE activity must be characterized for every speed set-point, which is an unfeasible approach in practical applications.

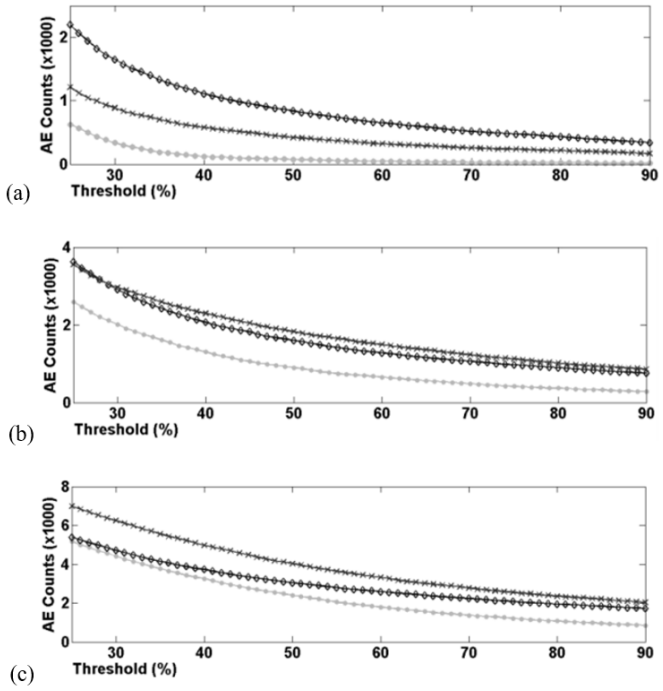

Fig. 6. Counting results of the AE events for the considered experimental tests during one rotation cycle under: *He* gear condition, ●; *Fa* gear condition, ◊; *Fb* gear condition, ×. (a) @ 150rpm. (b) @ 250rpm. (c) @450rpm.

Hence, in order to exploit hidden characteristic fault patterns in the AE signal under different gear conditions, the proposed method includes frequency analysis. The healthy gear condition is considered, first, to define the reference. In order to analyze the generalization capabilities of the method, all the AE data corresponding to the three gear conditions, *He*, *Fa* and *Fb*, at 250 rpm has been set apart. Thus, the data in regard with the 250 rpm operating condition is reserved just for testing purposes and will not be used during the training of the proposed method. The AE signals corresponding to the healthy gear condition at 150 rpm and 450 rpm are, then, decomposed in IMFs. Since the characteristics of the measured AE waveforms (amplitude and frequency distribution), reflect the presence of fractures in the gear teeth, the chromatic analysis of the resulting IMFs is proposed.

The first three IMF have been selected, which contain most part of the spectral band of interest for this application. Thus, it can be seen in Fig. 7 and Fig. 8 an example of time-based AE signal and IMFs under

healthy, *He*, and faulty, *Fb*, gear conditions at 150 rpm respectively, as well as the corresponding frequency distributions. Also, it can be seen in Fig. 9 and Fig. 10 an example of time-based AE signal and IMFs under healthy, *He*, and faulty, *Fb*, gear conditions at 450 rpm respectively, as well as the corresponding frequency distributions. Indeed, the EMD highlights the AE signal characteristics dealing with fractured teeth gears. It can be seen in Fig. 8(f) and Fig 10(f), the first IMF corresponding to the faulty, *Fb*, gear condition at 150 rpm, and at 450 rpm, respectively. In these two scenarios the contents differ, in terms of amplitude and frequency distribution of the homologous healthy condition, Fig. 7(f) and Fig. 9(f).

The amplitude of the acquired AE signals is highly related with the considered rotating speeds. However, compared with homologous healthy gear scenarios, the presence of fractures in the gear teeth introduces persistent alterations in the AE signature, including uneven frequency distributions and the extension of frequencies to higher parts of the considered bandwidth. Although second and third IMFs contain lower frequency bands, it can be observed also differences in their contents comparing healthy and faulty conditions.

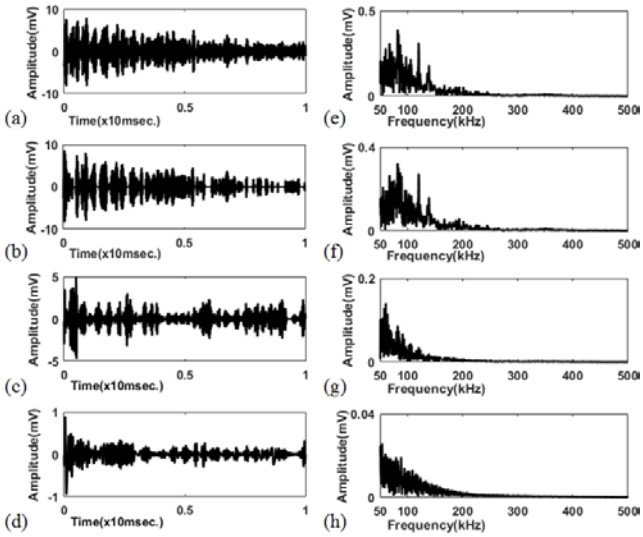

Fig. 7. Example of AE signal acquisition and resulting IMFs. Healthy gear condition @150rpm. (a) Time-based representation. (b) First IMF, time-based representation. (c) Second IMF, time-based representation. (d) Third IMF, time-based representation. (e) Frequency distribution. (f) First IMF,

frequency distribution. (g) Second IMF, frequency distribution. (h) Third IMF, frequency distribution.

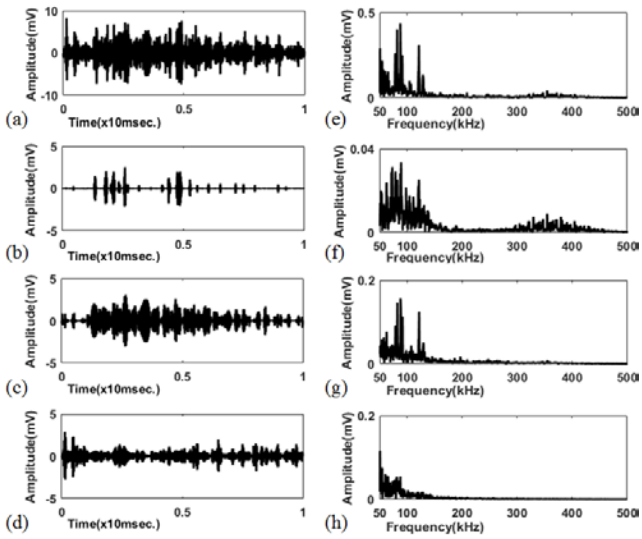

Fig. 8. Example of AE signal acquisition and resulting IMFs. Faulty, Fb, gear condition @150rpm. (a) Time-based representation. (b) First IMF, time-based representation. (c) Second IMF, time-based representation. (d) Third IMF, time-based representation. (e) Frequency distribution. (f) First IMF, frequency distribution. (g) Second IMF, frequency distribution. (h) Third IMF, frequency distribution.

In order to quantify such gear fracture affectations, the estimation of the chromatic parameters, *H*, *L* and *S*, over each considered IMF is proposed as suitable approach.

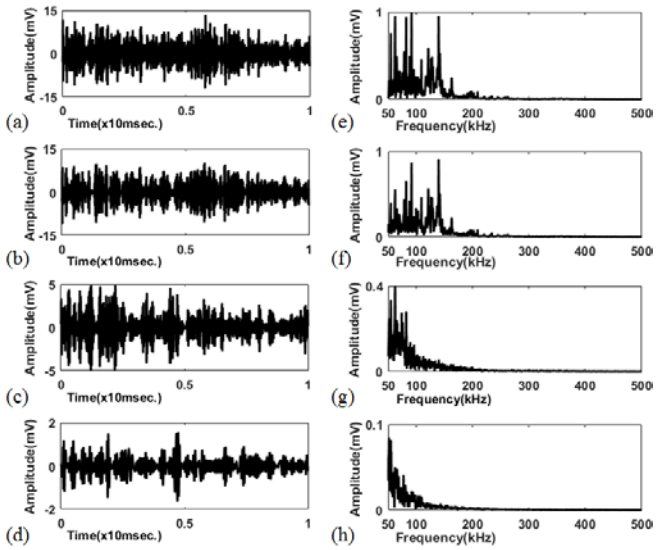

Fig. 9. Example of AE signal acquisition and resulting IMFs. Healthy gear condition @450rpm. (a) Time-based representation. (b) First IMF, time-based representation. (c) Second IMF, time-based representation. (d) Third IMF, time-based representation. (e) Frequency distribution. (f) First IMF, frequency distribution. (g) Second IMF, frequency distribution. (h) Third IMF, frequency distribution.

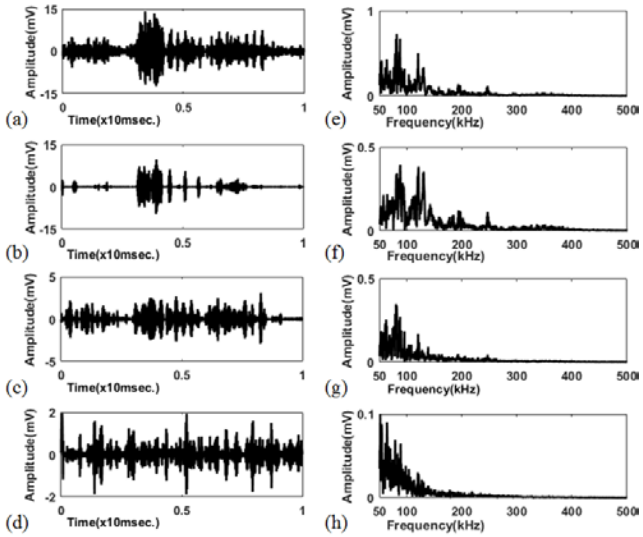

Fig. 10. Example of AE signal acquisition and resulting IMFs. Faulty, Fb, gear condition @450rpm. (a) Time-based representation. (b) First IMF, time-based representation. (c) Second

IMF, time-based representation. (d) Third IMF, time-based representation. (e) Frequency distribution. (f) First IMF, frequency distribution. (g) Second IMF, frequency distribution. (h) Third IMF, frequency distribution.

That is, for each IMF, three chromatic processors are applied to obtain the corresponding chromatic parameters. Three digital band-pass FIR filters with identical 225 kHz bandwidth have been designed with an overlapping of 50%, as a good tradeoff between simplicity and performance. The performances of the designed chromatic processors are shown in Fig. 11.

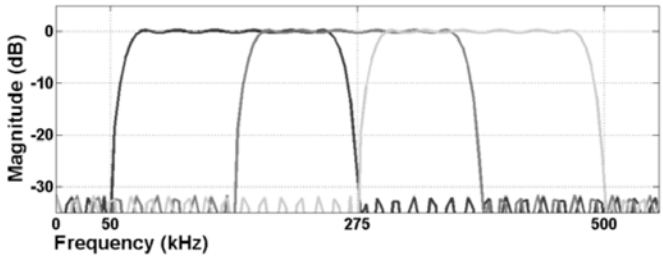

Fig. 11. Performance of the three proposed chromatic processors to be applied over each of the considered IMFs.

Thus, from each AE measurement, the three first IMFs are estimated and, for each of them, three chromatic processors are computed, resulting in a total of D=9 chromatic features, which compose the chromaticity space. In order to analyze the intrinsic dimension of data, that is, the minimum number of dimensions to maintain most of the data integrity, some estimators has been selected, such as geodesic minimum spanning tree (GMST), the principal component analysis (PCA), and the maximum likelihood (MLE), since each of them shows different estimation criteria [31]. Table I shows the intrinsic dimension estimation over the 9-space defined by the healthy data. Taking into consideration the non-orthogonality of the chromatic processors, an intrinsic dimensionality estimation lower than D is expected. In this sense,

SOM application results highly advantageous. On one hand, it quantizes the input data using model vectors in order to reach a discrete characterization of the D-dimensional manifold. On the other hand, it also performs a nonlinear projection to the units defined in a lower-dimensional map grid in order to be used as a visualization tool of the *D*-dimensional data representation.

TABLE I

INTRINSIC DIMENSION ANALYSIS OF THE *D*-DIMENSIONAL MANIFOLD

Estimator	Estimated intrinsic dimension
GMST	5.5665
PCA	5.0000
MLE	5.2285

As it has been mentioned, the SOM training has been carried out by the data corresponding to the healthy gear condition under 150 rpm and 450 rpm. A 2-dimensional grid of 25x25 neuron units has been defined as low-dimensional SOM representation. Thus, the model vectors corresponding to the 625 neurons units are adapted during the SOM training process, in this study, following a classical sequential training algorithm. The training process results a quantization error, Q_{error}, of 0.050, that is, the mean distance between each 9-dimensional data points and the corresponding (closest), 2-dimensional neuron units. This is a good data mapping resolution value considering that healthy 9-dimensional data dispersion is estimated at 0.5 approximately. In Fig. 12, a qualitative representation of the nine-dimensional chromaticity manifold is shown by means of the principal component analysis. The considered three principal components exhibit an accumulative variance of 72%, which emphasizes the qualitative meaning of the illustration. Two clusters can be identified in the data distribution, related with the affectation of the speed conditions considered (150 rpm and 450 rpm). It must be noted that, as the acquisition time is predefined, the gear's

teeth considered in each acquisition varies from one acquisition to another. This fact is also affected by the consideration of different rotating speeds. That consideration implies a certain degree of variance for each AE measurement and, in consequence, in each of the nine chromatic parameters.

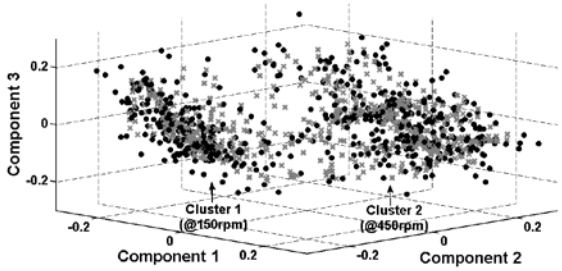

Fig. 12. Qualitative representation of the nine-dimensional chromaticity manifold by means of a 3-dimensional PCA based representation. Projection of healthy gear condition data @150rpm and 450rpm, ○. SOM neuron units' projection after training, ×.

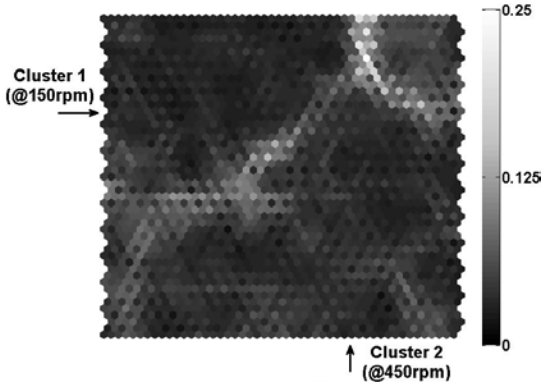

Fig. 13. Resulting U-matrix by means of the healthy gear condition data @150 rpm and 450 rpm. The lighter the color between two neuron units is, the larger is the relative distance between them.

The unified distance matrix method, U-matrix, applied over the resulting SOM training structure, allows the visualization of distances between adjacent neuron units in the defined two-dimensional map. It is shown in Fig. 13 that two main large areas can be distinguished, which means that the data behaves as two neighbor clusters. Indeed, the AE, as it was expected, exhibits speed modulations (150rpm and 450rpm in this case), considered in the chromatic characterization, mainly by the *L* parameter, of the proposed methodology. The component plane representation, Fig. 14, shows the individual component behaviors. Each plane shows the distribution of one of the chromaticity manifold dimensions. The components planes have been scaled in order to allow comparison. Component 1, Fig.14(a), *H* chromatic parameter, shows a predominance of the low frequency components in the AE signal under healthy gear condition. It can be seen that components 2, Fig.14(b) and 5, Fig.14(e), corresponding to the L chromatic parameter, exhibit a significant contrast between two regions of the corresponding component planes. This effect is due to the two rotating speed values considered and the consequence amplitude affectation, as it was aforementioned. Components 3, Fig.14(c), 6, Fig.14(f) and 9, Fig.14(g), corresponding to the *S* chromatic parameter, show an homogenous behavior, since the frequency distribution under healthy gear condition does not present relevant high frequency components.

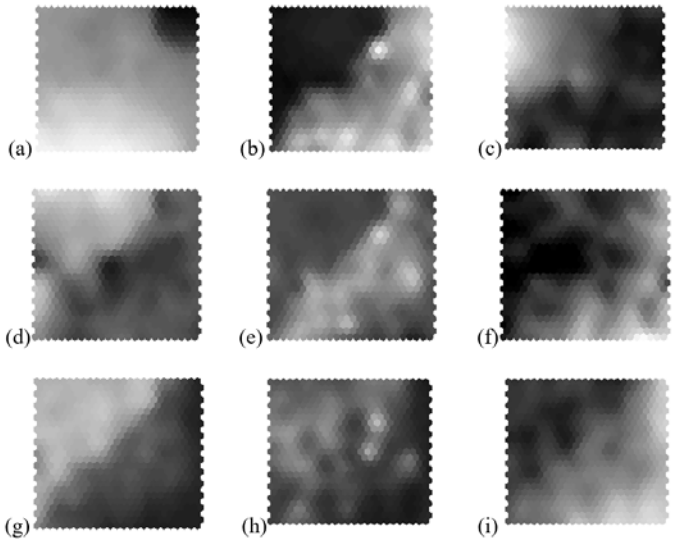

Fig. 14. Nine component planes of the resulting nine-dimensional chromaticity manifold model by SOM. Healthy gear condition data at 150 and 450rpm are considered. The lighter the color is, the higher the value of the component. (a) *H* of first IMF. (b) *L* of first IMF. (c) *S* of first IMF. (d) *H* of second IMF. (e) *L* of second IMF. (f) *S* of second IMF. (g) *H* of third IMF. (h) *L* of third IMF. (i) *S* of third IMF.

The data histogram of a new set of healthy data at 150 rpm and 450 rpm over the SOM training structure is shown in Fig. 15(a). It exhibits the data distribution in terms of hits over the neuron units. As expected, some neuron units are not selected as best matching units, however the histogram shows a proper homogeneous distribution over the SOM map.

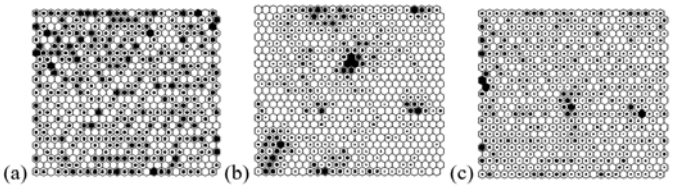

Fig. 15. Resulting data histogram of AE measurements collected during different gear conditions, including both speeds 150 rpm and 450 rpm. Larger the black square is, the larger is the number of matched measurements. (a) *He* gear condition. (b) *Fa* gear condition. (c) *Fb* gear condition.

Considering the trained SOM mapping with healthy data, the projection of the faulty gear conditions follows. This step has been done by the application of the same procedure, that is, EMD processing over the AE measurements, chromatic processors estimation, HLS transformation and, finally the projection over the trained SOM map. The resulting data histograms are shown in Fig 15(b) and Fig. 15(c) corresponding to *Fa* and *Fb* respectively. The projected AE measurements, corresponding to faulty gear conditions exhibit both healthy and faulty AE characteristics, since the gears are not homogeneously degraded. That is, some tooth has been induced to fracture while the rest still maintain their mechanical

properties. This is clear in the corresponding histograms representations. Unlike the healthy gear condition, the faulty scenarios show clusters of AE activity as well as a relative increase ratio of AE events at the boundaries of the reference map. The resulting quantization error corresponding to each AE measurement under the three considered gear conditions is shown in Fig. 16. Compared with the healthy gear data, Fig. 16(a), the deviation of some AE measurements under *Fa* and *Fb* gear conditions, Fig. 16(b) and Fig. 16(c) respectively, is explicit. The healthy gear condition exhibits a Q_{error} mean value of 0.52, that is similar to the one obtained during the SOM training stage, and a Q_{error} kurtosis value of 129.5, which means that a great deal of measurements are near the mean value. The *Fa* and *Fb* gear conditions, however, show Q_{error} mean values of 0.088 and 0.082 respectively, and Q_{error} kurtosis values of 31.10 and 7.73 respectively.

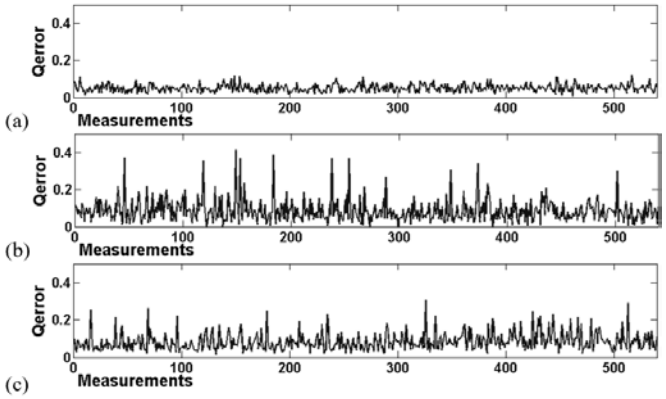

Fig. 16. Quantization error series resulting from the projection of AE measurements collected during different gear conditions @150 rpm and 450rpm. (a) *He* gear condition. (b) *Fa* gear condition. (c) *Fb* gear condition.

The presence of such AE faulty gear characteristics is quantified following the proposed gear mechanical degradation indicator, I_{GMD} (7). In order to avoid false positives, the healthy threshold, *Ht*, can be selected four times the Q_{error} mean value obtained during the SOM training, that is, in this study $Ht = 0.2$. Thus, while the healthy gear condition exhibits an $I_{GMD} = 0$, the *Fa* and *Fb* gear conditions show an $I_{GMD} = 6.2$

and an I_{GMD} = 4.6 respectively. Indeed, the *Fa* and *Fb* gear conditions contain different AE characteristics, due to the induced gear fractures, which differ from those corresponding to the healthy gear condition. Component 1, Fig. 17(a), *H* chromatic parameter, shows an increase of higher values compared with the homologous healthy gear condition. That is, an extension of the corresponding frequency distribution to higher frequency bands is observed. Components 2, Fig. 17(b), 5, Fig. 17(e) and 8, Fig. 17(h) corresponding to the *L* chromatic parameter, exhibit also a significant contrast between two regions of the corresponding component planes. Similar than in the healthy gear condition, this effect is due to the two rotating speed values considered. Components 3, Fig. 17(c), 6, Fig. 17(f) and 9, Fig. 17(g), corresponding to the *S* chromatic parameter, show an increase of lower values, since the frequency distribution under faulty gear condition presents additional high frequency components.

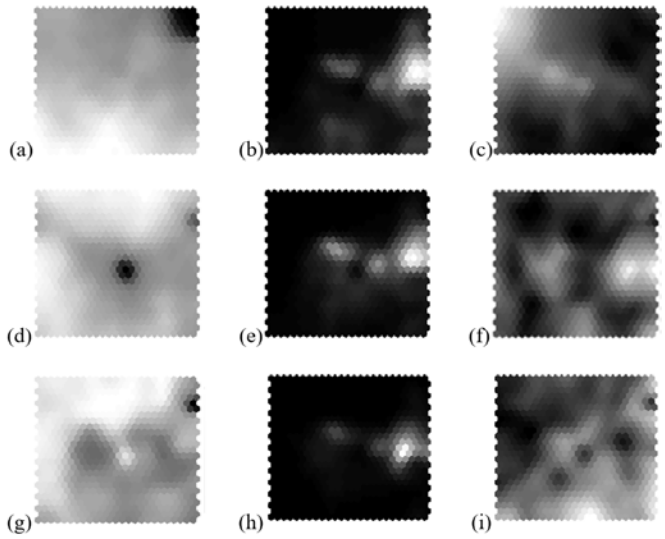

Fig. 17. Nine component planes of the SOM trained by means of faulty gear conditions data, *Fa* and *Fb*, at 150 rpm and 450 rpm. The lighter the color is, the higher the value of the component. (a) Parameter *H* of first IMF. (b) Parameter *L* of first IMF. (c) Parameter *S* of first IMF. (d) Parameter *H* of second IMF. (e) Parameter *L* of second IMF. (f) Parameter *S* of second IMF. (g) Parameter *H* of third IMF. (h) Parameter L of third IMF. (i) Parameter S of third IMF.

For checking the generalization and robustness properties of the proposed methodology, sets of AE measurements under each of the considered gear conditions, *He*, *Fa* and *Fb* at 250 rpm have been evaluated. The corresponding data histogram and quantization error is shown in Fig. 18 and Fig. 19 respectively. Under this new operating condition the healthy gear maintains an $I_{GMD} = 0$, and the *Fa* and *Fb* gears show an $I_{GMD} = 8.7$ and an $I_{GMD} = 4.9$ respectively.

The results show an excellent performance of the proposed methodology, allowing gear mechanical degradation detection under multiple speed conditions at a demanding low-load scenario. It must be noted that, for such range of operating conditions, no speed and torque measurements are required, however, for a wider range, the measurement of the speed and torque would be necessary. Thus, depending on the operating condition, a different chromaticity space would be applied.

The gear mechanical degradation indicator and, therefore, a possible threshold to pull out the gears to service for maintenance operation purposes can be specified by analyzing the trend of the I_{GMD} values depending of operating conditions. The analysis of the evolution of such indicator and the comparison with the values obtained from a healthy machine may indicate the value of this threshold.

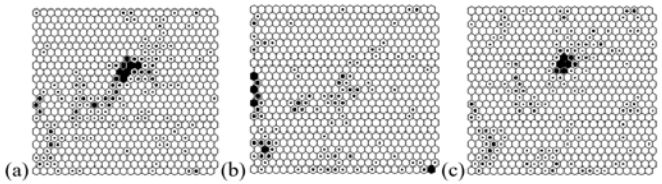

Fig. 18. Resulting data histogram of AE measurements collected during the three different gear conditions @250rpm. Larger the black square is, the larger is the number of matched measurements. (a) *He* gear condition. (b) *Fa* gear condition. (c) *Fb* gear condition.

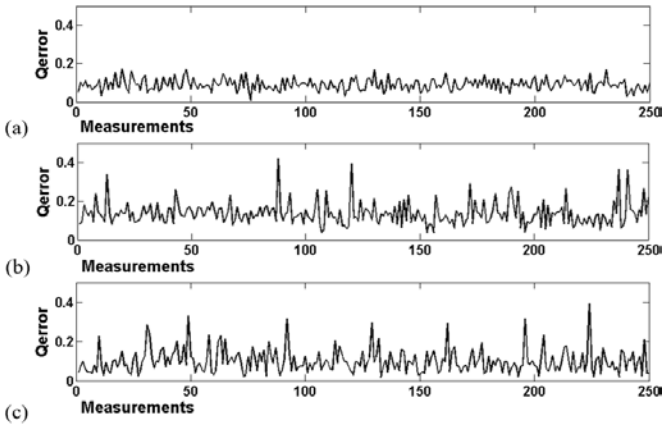

Fig. 19. Quantization error series resulting from the projection of AE measurements collected during the three different gear conditions @250rpm. (a) Healthy gear condition. (b) *Fa* gear condition. (c) *Fb* gear condition.

V. CONCLUSION

This paper presents a novel methodology in order to detect mechanical gear degradation in electromechanical systems under multiple speed operating conditions. There are three important aspects in this new method. The first one is the application of HLS transformation as a chromatic processing tool together with the AE analysis. HLS transformation offers a characterization of the amplitude and frequency distribution of the AE signal; highly suitable in case of gear mechanical degradation analysis. The second is the decomposition of the AE signal in IMFs, since the separation of the main different frequency modes allows the analysis of characteristic patterns. The third is the calculation of a new coefficient from the information provided by the HLS transformation of the main AE intrinsic mode functions by means of SOM mapping. Nine different experimental conditions have been considered, which represent an important range of system conditions. Under all of these experimental scenarios, the proposed fault indicator exhibit a reliable fault detection. Moreover, the gear mechanical conditions dealt with in the experimental tests represent noncritical gear faults. Therefore, the fault indicator shows still enough dynamic range to detect even lower gear mechanical degradation faults. The proposed feature estimation method exhibit a reliable

gear damage detection, since allows interpreting the underlying physical phenomenon of the mechanical degradation, that is, the differences in the amplitude and frequency distributions of the AE when mechanical gear fractures take place. It has to be highlighted that the proposed methodology is simple to implement. That is, it requires only the healthy data of the system and it shows a high reliability when performing the mechanical gear fracture detection in a range of speed operating conditions. The results obtained in this work suggest that this fault indicator may be also useful for any other rotating mechanical component faults. Future work will focus in the analysis of the load effect over the chromaticity space, and the optimum chromatic monitoring configuration in front of different gear fault types by means of AE signatures analysis.

ACKNOWLEDGMENT

The authors would like to thank the Fundació CTM Centre Tecnològic, Advanced Technological Centre in Catalonia, Spain, for the help during the mechanical gear fractures induction.

REFERENCES

[1] G.-A. Capolino, J. A. Antonino-Daviu and M. Riera-Guasp, "Modern Diagnostics Techniques for Electrical Machines, Power Electronics, and Drives," *IEEE Trans. Ind. Electron.*, vol. 62, DOI: 10.1109/TIE.2015.2391186, no. 3, pp. 1738-1745, Mar. 2015.

[2] H. Henao, G.-A. Capolino, M. Fernandez-Cabanas, F. Filippetti, C. Bruzzese, E. Strangas, R. Pusca, J. Estima, M. Riera-Guasp and S. Hedayati-Kia, "Trends in Fault Diagnosis for Electrical Machines: A Review of Diagnostic Techniques," *IEEE Ind. Electron. Mag.*, vol. 8, DOI: 10.1109/MIE.2013.2287651, no. 2, pp. 31-42, Jun. 2014.

[3] S. H. Kia, H. Henao and G.-A. Capolino, "Gear Tooth Surface Damage Fault Detection Using Induction Machine Stator Current Space Vector Analysis," *IEEE Trans. Ind. Electron.*, vol. 62, DOI: 10.1109/TIE.2014.2360068, no. 3, pp. 1866-1878, Mar. 2015.

[4] A. Garcia-Perez, R. de Jesus Romero-Troncoso, E. Cabal-Yepez and R. A Osornio-Rios, "The Application of High-Resolution Spectral Analysis for Identifying Multiple Combined Faults in Induction Motors," *IEEE Trans. Ind. Electron.*, vol. 58, DOI: 10.1109/TIE.2010.2051398, no. 5, pp. 2002-2010, May 2011.

[5] V. Sharma and A. Parey, “A Review of Gear Fault Diagnosis Using Various Condition Indicators,” *Procedia Engineering*, vol. 144, DOI: 10.1016/j.proeng.2016.05.131, pp. 253-263, 2016.

[6] Y. Qu, D. He, J. Yoon, B. Van Hecke, E. Bechhoefer and J. Zhu, “Gearbox Tooth Cut Fault Diagnostics Using Acoustic Emission and Vibration Sensors — A Comparative Study,” *Sensors*, vol. 14, DOI:10.3390/s140101372, no. 1, pp. 1372-1393, Jan. 2014.

[7] L. Zhang, D. Ozevin, W. Hardman, S. Kessler and A. Timmons, “Fatigue crack growth monitoring of idealized gearbox spline component using acoustic emission,” in Proc. *SPIE Smart Structures and Materials + Nondestructive Evaluation and Health Monitoring*, Las Vegas, United States, DOI:10.1117/12.2220163, pp. 409–411, 2016.

[8] E. Martinez-Gonzalez, “Detection of Failure Mechanisms of Tool Steels by means of Acoustic Emission Technique,” Ph.D. dissertation, Mechanics Engineering Dept., Technical university of Catalonia, Spain, 2014.

[9] E. Martinez-Gonzalez, I. Picas, D. Casellas and J. Romeu, “Detection of crack nucleation and growth in tool steels using fracture tests and acoustic emission,” *Meccanica*, vol. 50, DOI:10.1007/s11012-013-9858-9, n. 5, pp. 1155-1166, May 2015.

[10] Z. Shi, J. Jarzynski, S. Bair, S. Hurlebaus and L. J. Jacobs, “Characterization of acoustic emission signals from fatigue fracture,” *J. Mech. Eng. Sci.*, vol. 214, DOI: 10.1243/0954406001523588, pp. 1141-1149, 2000.

[11] M. Elforjani and D. Mba, A. Muhammad and A. Sire, “Condition monitoring of worm gears,” *Appl. Acoust.*, vol. 73, DOI: http://doi.org/10.1016/j.apacoust.2012.03.008, no. 8, pp. 859-863, Aug. 2012.

[12]C. K. Tan, P. Irving, and D. Mba, “A comparative experimental study on the diagnostic and prognostic capabilities of acoustics emission, vibration and spectrometric oil analysis for spur gears,” in *Mech. Syst. Signal Process.*, vol. 21, DOI: http://doi.org/10.1016/j.ymssp.2005.09.015, no. 1, pp. 208–233, Jan. 2007.

[13]R. Li and D. He, "Rotational Machine Health Monitoring and Fault Detection Using EMD-Based Acoustic Emission Feature Quantification," *IEEE Trans. Instrum. Meas.*, vol. 61, DOI: 10.1109/TIM.2011.2179819, no. 4, pp. 990-1001, Apr. 2012.

[14]M. Amarnath and I. R. Praveen Krishna, "Empirical mode decomposition of acoustic signals for diagnosis of faults in gears and rolling element bearings," *IET Sci. Meas.. Technol.*, vol. 6, DOI: 10.1049/iet-smt.2011.0082, no. 4, pp. 279-287, Jul. 2012.

[15]B. Eftekharnejad and D. Mba, “Use of advanced signal processing technique for analyzing the Acoustic Emission signatures from mechanical transmissions,” *in Proc. European Conf. Acoust. Emission Testing*, Vienna, Austria, Sep. 2010.

[16]D. Bianchi, E. Mayrhofer, M. Groschl, G. Betz and A. Vernes, “Wavelet packet transform for detection of single events in acoustic emission signals,” *Mech. Syst. Signal Process.*, vol. 64, DOI: http://doi.org/10.1016/j.ymssp.2015.04.014, pp. 441-51, Dec. 2015.

[17]G. R. Jones, P. C. Russell, A. Vourdas, J. Cosgrave, L. Stergioulas and R. Haber, “The Gabor transform basis of chromatic monitoring,” *Meas. Sci. Tech.*, vol. 11, DOI: https://doi-org.recursos.biblioteca.upc.edu/10.1088/0957-0233/11/5/307, no. 5, pp. 489-98, May 2000.

[18]A. G. Deakin, J. W. Spencer, D. H. Smith, D. Jones, N. Johnson and G. R. Jones, "Chromatic Optoacoustic Monitoring of Transformers and Their Onload Tap Changers," in *IEEE Transactions on Power Delivery*, vol. 29, DOI: 10.1109/TPWRD.2013.2294952, no. 1, pp. 207-214, Feb. 2014.

[19]A. G. Deakin, I. Rallis, J. Zhang, J. W. Spencer and G. R. Jones, “Towards holistic chromatic intelligent monitoring of complex systems,” *Sensor Rev.*, vol. 26, DOI: 10.1108/02602280610640616, no. 1, pp. 11-17, 2006.

[20]L. K. Stergioulas, A. Vourdas and G. R. Jones, “Gabor representation of optical signals using a truncated von Neumann lattice and its practical implementation,” *Opt. Eng.*, vol. 39, DOI:10.1117/1.602582, no. 7, pp. 1965-1971, 2000.

[21]E. Martínez González. “Detection of failure mechanisms of tool steels by means of acoustic emission technique,” Ph.D. dissertation, Technical university of Catalonia, Barcelona, January 2014.

[22]R. Pullin, A. Clarke, M. J. Eaton, M. R. Pearson, and K. M. Holford, “Identification of the onset of cracking in gear teeth Using acoustic emission,” in *Journal of Physics: Conference Series*, vol. 382, DOI: 10.1088/1742-6596/382/1/012050, no. 1, p. 12050, 2012.

[23]Y. Qu, J. Zhu, D. He, B. Qiu and E. Bechhoefer, "Development of a new acoustic emission based fault diagnosis tool for gearbox," *in Proc. IEEE Conf. Prognos. Health Manag.*, DOI: 10.1109/ICPHM.2013.6621418, pp. 1-9, Milan, Italy, Jun. 2013.

[24]E. H. S. Diop, R. Alexandre and A. O. Boudraa, "Analysis of Intrinsic Mode Functions: A PDE Approach," *IEEE Signal Process. Lett.*, vol. 17, DOI: 10.1109/LSP.2009.2038770, no. 4, pp. 398-401, Apr. 2010.

[25]D. P. Mandic, N. u. Rehman, Z. Wu and N. E. Huang, "Empirical Mode Decomposition-Based Time-Frequency Analysis of Multivariate Signals: The Power of Adaptive Data Analysis," in *IEEE Signal Processing Magazine*, vol. 30, DOI: 10.1109/MSP.2013.2267931, no. 6, pp. 74-86, Nov. 2013.

[26]N. E. Huang, Z. Shen, S. R. Long, M. C. Wu, H. H. Shih, Q. Zheng, N.-C. Yen, C. C. Tung, and H. H. Liu, “The empirical mode decomposition and the Hilbert spectrum for nonlinear and non-stationary time series analysis,” *in Proc. R. Soc. A Math. Phys. Eng. Sci.*, vol. 454, DOI: 10.1098/rspa.1998.0193, no. 1971, pp. 903–995, Mar. 1998.

[27]Z. Zhang, J. Wang and H. Zha, "Adaptive Manifold Learning," *IEEE Trans. Pattern Anal. Mach. Intell.*, vol.34, DOI: 10.1109/TPAMI.2011.115, no. 2, pp. 253-265, Feb. 2012.

[28]R. Li, S. U. Seçkiner, D. He, E. Bechhoefer and P. Menon, "Gear Fault Location Detection for Split Torque Gearbox Using AE Sensors," in *IEEE Transactions on Systems, Man, and Cybernetics, Part C*

(Applications and Reviews), vol. 42, DOI: 10.1109/TSMCC.2011.2182609, no. 6, pp. 1308-1317, Nov. 2012.

[29]B. Eftekharnejad, “Condition monitoring of gearboxes using Acoustic Emission,” Ph.D. dissertation, School of Enginnering, Cranfield University, Cranfield, Unied Kingdom, 2010.

[30]D. Yang, Y. Liu, S. Li, X. Li and L. Ma, “Gear fault diagnosis based on support vector machine optimized by artificial bee colony algorithm”, in *Mechanism and Machine Theory*, vol. 90, DOI: http://doi.org/10.1016/j.mechmachtheory.2015.03.013, pp. 219-229, August 2015.

[31]L.J.P. van der Maaten, E.O. Postma and H.J. van den Herik, “Dimensionality reduction: a comparative review”, Tilburg University Technical Report, TiCC-TR 2009-005, 2009.

BIOGRAPHIES

M. Delgado Prieto (S’08-M'12) received the B.S., M.S. and Ph.D degrees in Electronics Engineering from the Universitat Politècnica de Catalunya, UPC, Barcelona, Spain in 2004, 2007 and 2012 respectively.

In 2008 he joined the MCIA Research Center at UPC, Terrassa, Spain, where he is currently a Research Director. His research and technology transfer activity include industrial systems monitoring and diagnosis, predictive maintenance, machine learning, signal processing methods and embedded systems.

D. Zurita Millan (S’13) received his M.S. degree in Electronics Engineering from the Universitat Politècnica de Catalunya, UPC, Barcelona, Spain, in 2013.

In 2013 he joined the MCIA Research Center at UPC, Terrassa, Spain, where he is currently developing his studies towards the Ph.D. degree in the Electronic doctoral program of the UPC. His research interests include fault diagnosis and prognosis of

electro-mechanical systems, industrial process monitoring, fault detection algorithms, machine learning and signal processing based methods.